X-Ray Absorption Spectroscopy Study of Battery Materials

Marco Giorgetti, Lorenzo Stievano

Chapter 4

X-Ray Absorption Spectroscopy Study of Battery Materials

Marco Giorgetti and Lorenzo Stievano

Additional information is available at the end of the chapter

http://dx.doi.org/10.5772/66868

Abstract

X-ray absorption spectroscopy (XAS) as a local structural tool for the study of the electrochemical processes in battery materials is highlighted. Due to its elemental specificity and high penetration of the X-rays in the 4–35 keV range, XAS is particularly suited for this, allowing the study of battery materials using specifically developed *in situ* electrochemical cells. This energy is required to dislodge one core electron from transition metal or p-group atoms, which are commonly used as redox centers in positive and negative electrode materials. In such a simple picture, the ejected photoelectron is scattered by the surrounding atoms, producing characteristic traces in the X-ray absorption spectrum. Both positive and negative electrode materials (intercalation, alloy and conversion electrodes) can be studied. The chapter starts with an introduction of the context around battery studies, followed by a short explanation of the photoelectric effect at the basis of the X-ray absorption phenomenon and to specific features of XAS. A selection of XAS experiments conducted in the field of batteries will be then outlined, also emphasizing the effects due to nanoscale dimension of the material studied. Finally, a perspectives section will summarize the specific role that this spectroscopy has played in the battery community.

Keywords: X-ray absorption spectroscopy, lithium batteries, energy materials, electrode materials

1. Introduction

One of the most challenging difficulties that our planet has to face in the next decades is the sustainable use of energy. In particular, the demand for advanced energy storage devices has increased significantly, motivated by a variety of different needs of our technologically driven, highly mobile, energy challenged society. For instance, batteries are the devices that can solve the problems inherent to the intrinsic intermittency of renewable energy sources, since they can store the energy surplus produced in excess when the plant is operating and then feed it to the power grid when

there is a peak of consumption. Moreover, they are also targeted to fulfill the ever growing demand of energy for portable applications (mobile phones and computers, and nowadays cars and trucks). The excellent performance and the well-established technology of lithium-ion batteries (LIBs) put them in a crucial position for supporting this new energy revolution. Several post-LIB systems, such as lithium-sulfur batteries (LSBs), lithium-oxygen batteries (LOBs) or sodium-ion batteries (NIBs), have also been proposed in the last years, as sustainable performing alternatives to LIBs.

Differently from other well-established battery technologies, such as alkaline or lead-acid batteries, LIBs (as well as the other post-LIB systems) are based on the famous "rocking chair" mechanism [2], where the Li^+ cations are exchanged alternatively between the positive and the negative electrode during the discharge and the charge process, as shown in **Figure 1**. In such a system, the two electrodes can be any sort of material that are able to undergo reversibly to a reduction/oxidation process at a specific high or low potential (for the positive or negative electrode, respectively) with the concomitant addition/elimination of Li^+ cations. For this reason, many materials able to form lithiated phases have been proposed for playing the role of electrode materials.

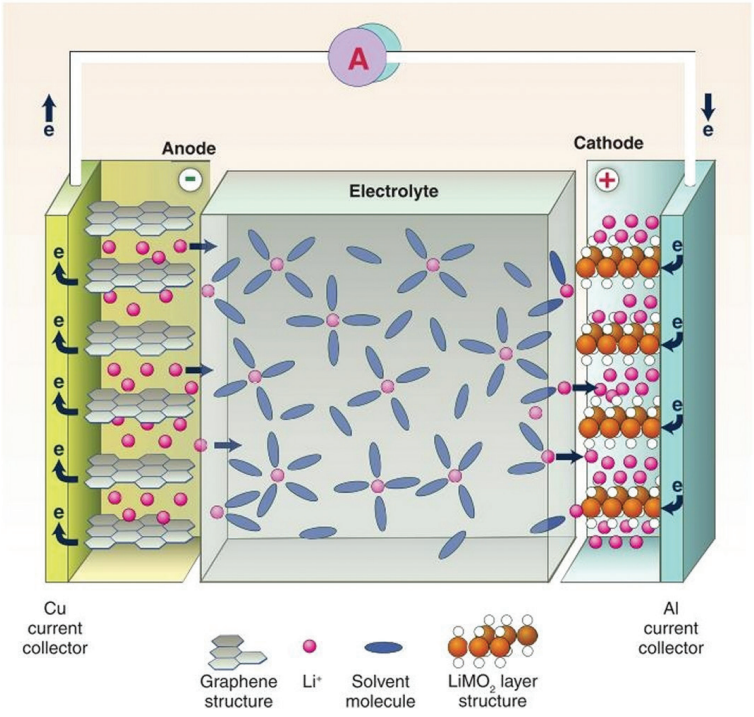

Figure 1. Schematic representation of the discharge of a Li^+-ion battery: a graphite-based negative electrode undergoes Li^+ deintercalation, according to the following reaction:.

$$\mathbf{Li_xC} \leftrightarrows \mathbf{C} + x\,Li^+ + x\,e^-$$

Li^+ ions migrate toward the $Li_{1-x}CoO_2$ positive electrode forming the reduced $LiCoO_2$:

$$Li_{1-x}CoO_2 + x\,Li^+ + x\,e^- \leftrightarrows LiCoO_2$$

Typical electrolytes are based on a lithium salt (*e.g.* $LiPF_6$) dissolved in a mixture of liquid carbonates (Ethylene carbonate, propylene carbonate, etc.) Reproduction from Ref. [1].

The very large number of possible host materials for Li^+ have generated a great deal of works on potential LIBs electrode materials, from the micro to the nanosized range, which may accommodate lithium via different reaction mechanisms, including intercalation [3–5], alloying [6–8] and conversion [9] reactions. In addition to the reaction mechanisms at the electrodes, other features concerning the electrolytes and their interaction with the electrodes, including the formation of the solid-electrolyte interphase (SEI) [10], which is of primordial importance for the stability and the cycle life of the battery, have been thoroughly studied.

In such a picture, many characterization methods have been proposed and efficiently used, either simply *ex situ*, *in situ* or under even *operando* conditions for the characterization of the starting materials and of their reaction mechanisms such as X-ray diffraction (XRD) [11], infrared [12], Raman [13], Mössbauer [14] and X-ray photoelectron spectroscopy [15, 16].

X-ray absorption spectroscopy (XAS) can also be counted among the characterization tools used in the field of batteries. Indeed, it is one of the techniques of choice for retrieving structural and electronic information, especially when the materials or some of the species formed through the electrochemical reactions are not crystalline and cannot be studied by diffraction techniques. The main important characteristics of XAS are: (i) its element specificity, which allows the study of a particular element by concentrating on its K (or in some cases L) absorption edge; (ii) the possibility of tuning it to different sites (for instance Fe and P in $LiFePO_4$), thus providing sources of complementary information on the same compound; (iii) the physico-chemical information contained in the near-edge structure of the XAS signals, which can be used to reveal the formal oxidation state and the local symmetry of the probed atom; (iv) the possibility of doing *operando* measurements by collecting XAS spectra during electrochemical cycling using specifically developed *in situ* cells. In this case, the physico-chemical properties and the local structure of the studied element can be monitored at all moments during the charge and discharge processes.

To the best of our knowledge, the first use of XAS in the field of batteries dates back to the paper of Mc Breen *et al.* [17]. Several reviews have appeared more recently, resuming the principal advances allowed by the application of XAS in this research field [18–21]. In this chapter, after a short presentation of the techniques and of the relative experimental methods, a selection of XAS experiments conducted in the field of batteries will highlight the potentiality of the technique in the *in situ* characterization of nanosized, nanostructured and badly organized materials. This knowledge is necessary to obtain a precise description of the electrochemical mechanisms governing battery's chemistry.

2. X-ray absorption spectroscopy (XAS)

XAS, also known as X-ray absorption fine structure (abbreviated as XAFS) spectroscopy, is a powerful tool that provides information on a very local scale (4–5 Å) around a selected atomic species and is well suited for the characterization of not only crystals but also materials that possess little or no long-range translational order. It is based on the absorption: when a sample

is exposed to X-rays, it will absorb part of the incoming photon beams, which is mainly generated by the photoelectric effect for energy in the hard X-rays regimes (3–50 KeV). XAS is even selective for the atomic species and also allows us to tune the X-rays beam selectively to a specific atomic core (the absorption energy of next elements are sufficiently spaced), and therefore it probes the local structure around only the selected element that are contained within a material. The element-specific characteristic of XAS, providing both chemical and structural information at the same time, differentiates it from other techniques, such as the X-ray scattering. In this respect, it serves as a unique tool for the investigation of battery materials during charge-discharge cycles.

XAS experiment measures the absorption coefficient μ as a function of energy E: as E increases, μ generally decreases ($\mu \sim E^{-3}$), that is matter becomes more transparent and X-rays more penetrating, save for some discontinuities, where μ rapidly rises up. These exceptions correspond to particular energies, the so-called absorption edges E_0, which are the characteristic of the material, where the amount of energy exactly matches the core electron binding energy. The edge energies vary with atomic number approximately as a function of Z^2 and both K and L levels can be used in the hard X-ray regime (in addition, M edges can be used for heavy elements in the soft X-ray regime), which allows most elements to be probed by XAS with X-ray energies between 4 and 35 keV. Because the element of interest is chosen in the experiment, XAFS is element-specific.

XAS (or XAFS) is generally used to refer to the entire spectrum, which is constituted by the edge region called X-ray absorption near edge spectroscopy (XANES), which is limited at the first 80–100 eV above the edge, and a post-edge region extended X-ray absorption fine structure (EXAFS), which is extended up to 1000 eV above the absorption edge. The distinction between XANES and EXAFS remains arbitrary, but some important approximations in the theory allow us to interpret the extended spectra in a more quantitative way than is currently possible for the near-edge spectra. The XANES region, comprising the pre-edge and the absorption edge itself, is strongly sensitive to oxidation state and coordination chemistry of the absorbing atom of interest. The EXAFS region has been largely exploited to gain quantitative structural information such as first shell distance of the metal site and the coordination number. EXAFS comprises periodic undulations in the absorption spectrum that decay in intensity as the incident energy increases well over (~1000 eV) the absorption edge. These undulations arise from the scattering of the emitted photoelectron with the surrounding atoms. A striking feature of XAFS is that this technique can be applied to all states of matter, and for both crystalline and amorphous materials, it has been used with great success in many research fields, such as liquids [22], catalysis [23–25], biology [26], inorganic metal complexes [27] and electrochemical interfaces [28]. Several excellent books are also available [29–32]. The website of the International XAFS society is reachable at http://www.ixasportal.net/ixas/.

When discussing XAS, we are primarily concerned with the absorption coefficient μ, which gives the probability that X-rays will be absorbed according to Beer's Law:

$$\mu \cdot x = \ln(I_0/I) \tag{1}$$

$$\left(\frac{\mu}{\rho}\right) \cdot \rho \cdot x = \ln(I_0/I) \tag{2}$$

being I_0 is the intensity of X-ray incident on a sample, x is the sample thickness and I is the intensity transmitted through the sample, as shown in **Figure 2**. The measured quantity, μ (cm^{-1}), is the linear X-ray absorption coefficient which is closely related to its inverse $1/\mu$ called the absorption length (cm). The absorption length is defined as the linear distance of the material over which the X-ray intensity results attenuated by a factor $1/e$ ~ 37%. This quantity is important in planning the experiment, as it sets the scale for choosing an appropriate sample thickness.

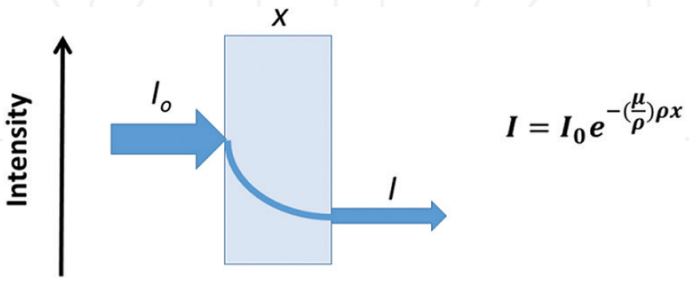

Figure 2. Sketch for the X-Ray absorption measurement in transmission mode.

Normalization to the density of the material results quite convenient, as different states of matter may be analyzed: the mass absorption coefficient μ_m (cm^2/g) is the linear absorption coefficient divided by the density of the absorber.

X-rays ionize and the absorbing atom turns to an excited ion after the electron liberation. Relaxation may occur in two different ways: (i) the core-hole may be filled by a higher-energy electron and the energy difference is released as a second photon, whose energy is smaller compared to that of the primary absorption, for an inner transition occurs (the detection of which is at the basis of another x-ray analytical technique, X-ray Fluorescence Spectroscopy—XFS) or (ii) an Auger secondary electron may be freed, after having absorbed the second photon. The measurement of these electrons is made possible by Auger spectrometers. In the soft X-ray region (<2 keV), the Auger process is more likely to occur, unlike for higher energies where X-ray fluorescence dominates.

2.1. Extended X-ray absorption fine structure (EXAFS)

When X-ray is absorbed by a core-level electron, a photoelectron with wavevector k is created and propagates away from the atom as a spherical wave as seen from the blue lines of **Figure 3**. The wavevector k is related to the excess of the energy $\hbar\omega$-E_0 of the incoming X-ray beam by:

$$k = \sqrt{\frac{2m}{\hbar^2}(\hbar\omega - E_0)} \tag{3}$$

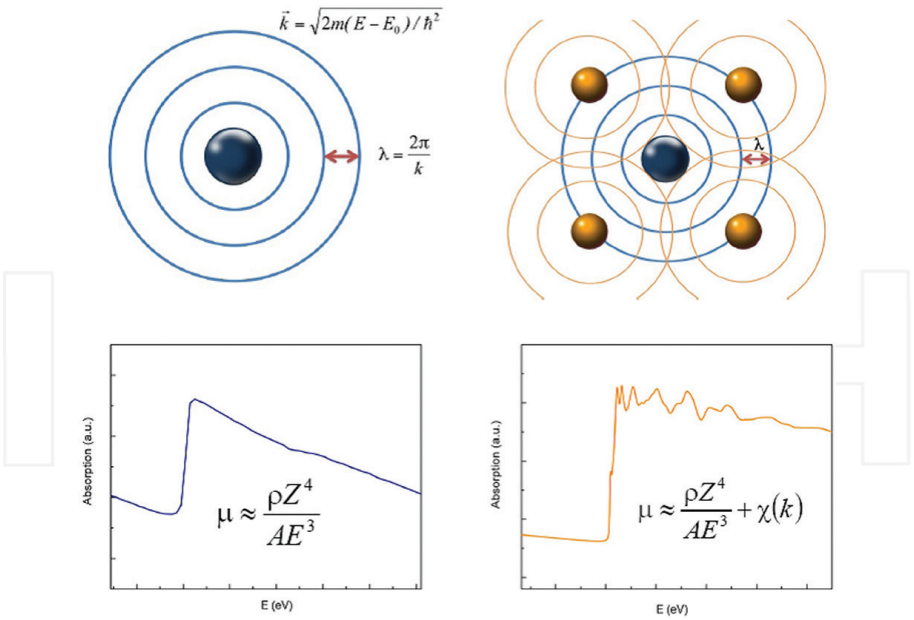

Figure 3. Emission of a photo-electron for an isolated (left) and a coordinated (right) atomic species. In the latter the absorption coefficient measured at a central atom threshold shows a fine structure due to the presence of neighboring atoms. Reproduced from Ref. [18].

where E_0 is the binding energy of the core-electron that is excited and $E = \hbar\omega$ is the energy of the absorbed x-ray photon. Thus, the excess of energy rules out the optical property of the photo-electron created by the photoabsorption process. In case of isolated atoms, the propagation is simply described by one wave going away from the atom and the absorption coefficient μ is described by a smooth function of energy, indicated in the lower panel of **Figure 3**. Its value depends on the sample density ρ, atomic number Z, atomic mass A and the X-ray energy E, roughly expressed as:

$$\mu_0 \approx \frac{\rho Z^4}{A E^3} \tag{4}$$

The appendix 0 indicates the value for an isolated atom. It is remarkable here that due to its Z^4 dependence, the absorption coefficients of different elements exhibit big discrepancies, (spanning several orders of magnitude) so a good contrast between different materials can be achieved for any sample thickness and concentrations by selecting the X-ray energy. This fact is at the origin of the X-rays imaging techniques based on contrast.

If other atoms are located in the vicinity of the absorber (the central atom), the photoelectron is scattered by the neighbors (yellow atoms) and so does every atom in the material. The incoming and the scattered wave interferes either constructively or destructively as a function of the energy of the X-ray beam. Therefore, the observed absorption coefficient is expected to vary periodically as a function of the energy as depicted at the bottom right of **Figure 3**. In the latter

case, the total absorption coefficient μ can be expressed as the isolated atomic absorption μ_0, modulated by a correction factor $\chi(E)$, the oscillation, which is also defined as the EXAFS signal:

$$\mu(E) = \mu_0(E)\left[1 + \chi(E)\right] \tag{5}$$

This allows one to extract the oscillations from a raw experimental spectrum:

$$\chi = \left[\left(\mu(E) - \mu_0(E)\right]\right/ \mu_0(E) \tag{6}$$

For practical purpose, the denominator is often replaced by $\mu_0(E_0)$, which is the atomic absorption evaluated at the edge energy. $\chi(k)$ can be considered as the fractional change in absorption coefficient induced by the presence of neighboring atoms.

Within this simple description, the EXAFS can be represented by an oscillation, which of course can be described by terms of amplitude and phase. In a first approximation, the amplitude term depends on the nature and the number of near neighbors around the central atoms and the phase on the mutual distance photoabsorber scatterer. This leads to a simple expression for EXAFS in terms of different parameters affecting the fine structure:

$$\chi(k) \sim \sum_j \frac{N_j F_j(k)}{k r_j^2} \sin\left[2k R_j + \delta(k)\right] \tag{7}$$

where N_j represents the coordination number of identical atoms at approximately the same distance r_j from the central atom. This group of atoms is called as a coordination shell and contributes to one components of the EXAFS signal. The peculiar $F_j(k)$ term is called the backscattering amplitude and depends on the nature of the scatterer atom. Different atom types have different backscattering amplitude. A crucial issue is given by the inverse quadratic dependence of the oscillation to the distance. This is due to the decay of the photoelectron as a function of time and distance and thus making the EXAFS a short-range structural probe. The first term of the phase $2kR_j$ is due to the geometrical phase shift suffered by the photoelectron with wavevector k on its trajectory twice the distance r_j between the photo absorber and the scatterer. In addition, as the electron is not moving in a constant potential, a phase shift $\delta(k)$ has to be added to this expression to account for the interaction of the electron with the varying potential of the absorbing and backscattering atom.

Several effects have to be taken into account to complete the description of real systems, and they all can be considered damping terms. They are (i) the structural and thermal disorder; (ii) the limited mean free path of the photoelectron; and (iii) the relaxation of all the other electrons in the absorbing atom in response to the hole in the core level. The first term is due to the fact that atoms in matter vibrate around their equilibrium position depending on temperature. This atomic motion reduces the EXAFS amplitude, and a term called the EXAFS Debye-Waller factor σ^2 is introduced. In EXAFS, this term corresponds to the mean square average of the difference of the displacement of the backscatterer relative to the displacement of the absorber. The second term is due to inelastic scattering processes of the photoelectron with other electron and thus an additional damping factor is introduced, where $\Lambda(k)$ is the

photoelectron mean free path (how far the electron travels before scattering inelastically). Finally, the amplitude reduction term S_0^2 accounts for the shake-up/shake-off processes of the central atom. Those processes (multi-excitations) refer to the excitations of the remaining $Z - 1$ "passive" electrons of the excited atom. This is a scale factor, and it is usually in the 0.7–1 range. By taking in consideration with these effects, the EXAFS equation becomes:

$$\chi(k) = \sum_j \frac{N_j F_j(k)}{k r_j^2} e^{-2k^2\sigma^2} e^{-2R_j/\Lambda(k)} S_0^2 \sin\left[2k R_j + \delta(k)\right] \tag{8}$$

This is valid for the plane wave approximation, *K* threshold, single scattering, single electron approximation and "sudden" approximation. A similar equation valid for the other edges (L_{III}, etc.) must be considered. The structural and non-structural parameters appearing in the equation sum up to compose the EXAFS spectrum. To access these parameters in an experimental EXAFS spectrum, a data analysis has to be performed. This procedure is time consuming and it should be considered the slow step of the overall XAFS methodology.

EXAFS data analysis is normally done by using code programs, which permit to calculate the theoretical EXAFS spectrum based on *ab initio* calculations, followed by a further step which compares the experimental signals to the theoretical ones (fitting procedures). A rather complete list of the available software can be found at: http://www.esrf.eu/Instrumentation/software/data-analysis/Links/xafs. Typical widely used computer programs are GNXAS [33], FEFF [34, 35] and EXCURV [36]. EXCURV is a program, which simulates EXAFS spectra using rapid curved-wave theory. GNXAS package is based on multiple-scattering (MS) calculations and a fitting procedure of the raw experimental data, also allowing multiple edge fittings and a non-Gaussian distribution models for the atoms pair distribution. FEFF allows MS calculations of both EXAFS and XANES spectra for atomic clusters. The code yields scattering amplitudes and phases used in many modern XAFS analysis codes. It is also linked to the IFEFFIT package [37, 38], a suite of interactive code for XAFS analysis, combining high-quality and well-tested XAFS analysis algorithms, tools for general data manipulation and graphical display of data.

Two more considerations should be made on EXAFS data analysis. The first is that XAS (and therefore the results obtained by an EXAFS analysis) is a bulk technique and thus all the atoms irradiated by the beam contribute to the overall XAS spectrum. The same is true in the case of a multicomponent system (for instance two phases in equilibrium of a polymorphic species). Each component or phase gives its contributions. An example to disclose the simple component of a species, such as in the case of gold nanoparticles and its precursors, appeared [39]. Alternatively, an efficient use of chemometry has been proposed for the analysis of XAS data in such cases [40]. This approach has interesting implication for the interpretation of spectra recorded during an *operando* acquisition and an example will be presented in the next section.

The second consideration concerns the EXAFS data analysis of nanoparticles and nanostructures [41, 42]. This issue has been addressed for metal nanoparticles first [43], evidencing that

http://dx.doi.org/10.5772/66868

by decreasing the size of the material there is a significant effect on the observed coordination number, due to the increased surface/bulk ratio. A specific example of this effect on a battery material will be presented in the case study section.

2.2. X-ray absorption near edge spectroscopy (XANES)

The XANES region is sensitive to the geometrical structure of the metal center but also probes its effective charge. It turns out that the position of the edge (which can be evaluated by the edge inflection point) is shifted to higher energies when the formal valence of the photo-absorber increases. Below the absorption edge, the presence of pre-edge structures can be observed [44]. The occurrence of this peak in a metal (first raw transition metal) K-edge is due to 1s-3d electronic transition [45] that is electric-dipole forbidden but quadrupole allowed. Its intensity can be used as a probe for geometry, as the geometrical distortion of the metal core from centrosymmetric coordination favors the transition, while the energy position is relative to the metal core formal oxidation state. This fact is frequently used for investigating the charge associated to positive- and negative-electrode materials during reduction and oxidation reactions in batteries.

If we now consider the form of the absorption edge, it can be seen that it reflects the empty density of states and it strongly depends on the coordination, while the forms of the absorption traces up to 60–80 eV are due to the multiple scattering resonances of the ejected photoelectron. Several computer codes can simulate the XANES spectrum, such as above-mentioned FEFF, MXAN [46], FDMNES [47] and CTM4XAS [48], which are useful for the analysis of metal L-edges.

3. Investigating a battery at work: *ex situ* and *in situ (operando)* studies

The simplest way to study the structural end electronic modification of a cathode or anode material is by *ex situ* XAS. XANES and EXAFS spectra at a selected K-edge are collected at a specific state of charge (or discharge) of the battery. In this case, the battery is stopped at the chosen state of charge (or discharge) and disassembled; the recovered material, protected from air in adapted sample holders, is transported to a synchrotron to perform the experiment in a suitable XAS beamline [32]. Basically, two geometries are used for this purpose, namely transmission and fluorescence. In transmission geometry, the sample is placed between I_0 and I detectors and the absorption is measured according to the Beer's law exponential decay, as mentioned before. The fluorescence detection is carried out by tilting the sample at 45 degrees and collecting the fluorescence X-rays by using a solid-state detector at the right angle with respect to I_0.

Such *ex situ* XAS studies of electrode materials are now extensively completed by *operando* measurements, *i.e.*, performed during a discharge or charge process. Such an approach allows one to avoid several drawbacks due to the sample transfer needed for the *ex situ* measurements. Alteration of air- or moisture-sensitive species is avoided, as well as the occurrence of relaxation reactions which might show up when the electrical circuit is open,

inducing a transformation of the unstable cycled material [49]. The effects of sampling deviations are also eluded since the sample remains in the same position during the whole measurement series. Finally, the whole study can be performed on a single test cell suppressing the effects of uncontrolled differences in a set of cells which are needed for a stepwise *ex situ* study of the electrochemical mechanism. To perform such an experiment, a special *in situ* electrochemical cell, obeying to the specific requirements of XAS, has to be used. This cell consists of an electrode containing the active material, a lithium foil, a separator, which is typically a polymeric membrane such as Celgard, and an electrolyte, usually based on organic carbonate solvents such as propylene carbonate (PC), dimethyl carbonate (DMC) and ethylene carbonate (EC).

Figure 4 displays two different types of *in situ* electrochemical cells. The first one (left) is a typical pouch cell which is characterized by a large dimension of the cathode. In this case, a film containing the active material is previously deposited on a square Al (or Cu) current collector of 4 cm^2 and assembled in a glove box together with a Li (Na) counter-electrode, a separator and the electrolyte. The mass loading varies between 2 and 15 g/cm^2 of active material, depending on the energy of the X-ray. Sometimes, a small tube (visible in the right part of the cell) can be used as a sink for the gas, which may be released during the electrochemical processes and which can be analyzed in line, if necessary. The figure on the right displays a typical stainless steel cell [50], which uses self-supported films or pellets of electrode material of smaller dimension (1 cm diameter). The versatility of this second approach is testified by the successfully use of this cell in transmission and fluorescence geometry, as well as in other techniques including *in situ* XRD [51], Mössbauer [52] and Raman spectroscopy [53] measurements.

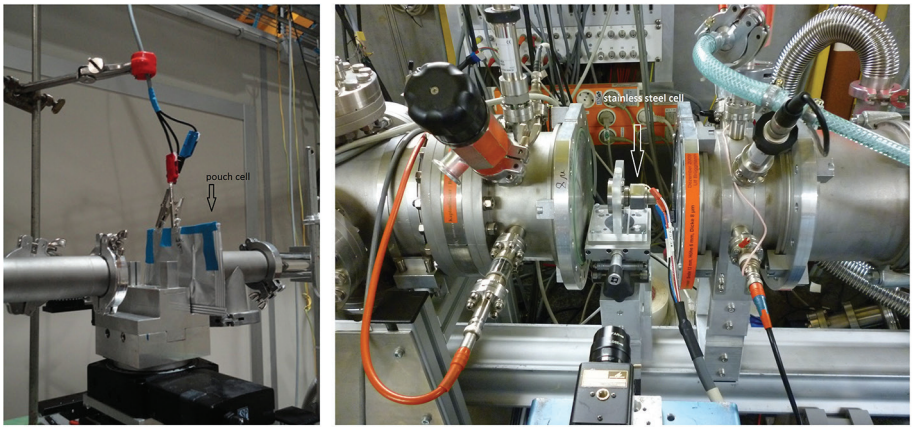

Figure 4. Typical *in situ* electrochemical cells used for *operando* XAS studies of batteries: A pouch cell (left) and a stainless steel cell (right) mounted on different XAS beamlines.

http://dx.doi.org/10.5772/66868

4. Case studies in battery materials

Given the large amount of physico-chemical information that it usually carries, already mentioned in the previous sections, XAS has been largely applied to the study of battery materials [18, 19]. A few particular case studies, specifying specific features of this technique in particular cases involving nanostructured species, are presented in the following paragraphs. It will be stressed, in particular, the importance of performing *in situ* studies compared to more simple, but also often less reliable, *ex situ* measurements.

4.1. *Ex situ* studies of lithium-excess manganese layered oxides

The relative abundance of manganese coupled with their variety of oxides structures, which provides generally a three-dimensional array of edge-shared MnO_6 octahedra for the lithium insertion and release, has aroused the interest of developing positive-electrode materials based on manganese oxide. Due to the well-known poor cycling capability of the spinel structure $LiMn_2O_4$, where a cooperative Jahn-Teller distortion of the Mn^{3+} ion causes a cubic-to-tetragonal phase transition leading to a rapid degradation of the electrode, an intensive research has been focused on alternative materials. Solid solutions of layered cathode materials such as the combination of Li_2MnO_3 and $LiMO_2$ (M = Mn, Co, Ni, etc.) have been proposed as promising candidates for cheaper, higher capacity and safer positive electrode for lithium batteries. However, the occurrence of an initial activation process during the first delithiation step (first charge) is always accompanied by a large irreversibility in terms of specific capacity. To gain a deeper understanding of the initial activation step and to study the following delithiation-lithiation process, an electronic and local structural characterization of the host material is required and the XAS is the technique of choice. A series of electrodes with different lithium concentration (state of charge, SOC) were studied in a series of lithium-rich, cobalt-poor $Li[Li_{0.2}Ni_{0.16}Mn_{0.56}Co_{0.08}]O_2$ electrode material (NMC), as an examples of *ex situ* XAS investigation [54, 55]. Due to the strong sensitivity of the XAS to the metal site, spectra at the three different metal edges can be measured, allowing the study of the evolution of the physico-chemical properties and of the local structure of each metal site.

Figure 5 shows the voltage profile of the cell during charge-discharge operation. The numbered points in the curve indicates predetermined states of charge (SOC) at which cells were prepared for the XAS measurements. **Figure 6** summarizes the XAS analysis conducted on the materials, where all the several portions of the X-ray absorption spectrum carry valuable information on the local and electronic structure: pre-edge, XANES and EXAFS. The pre-edge analysis (the Mn K-edge is displayed in the figure, showing two components) allowed the authors to check the variation of the Mn local site, in terms of symmetry and charge. XANES traces can provide the identification of the electroactive sites at different SOC and the EXAFS analyses the local structural information of the selected metal site. This information is complementary with respect to XRD which probes the long-range order in crystalline materials.

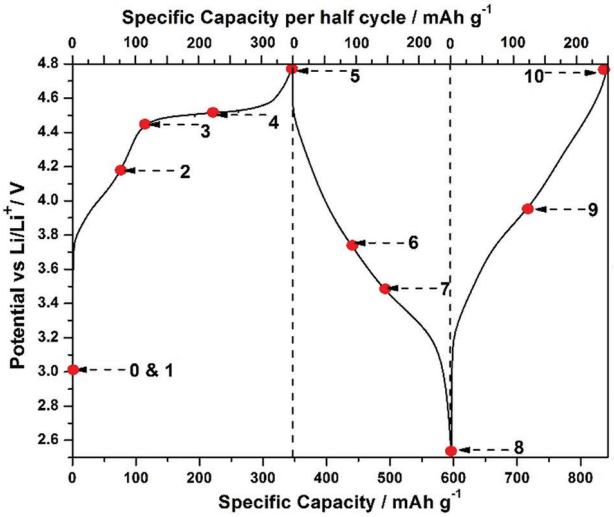

Figure 5. Voltage profile of two successive charge and discharge curves of Li-rich NCM at 20 mA/g. Representative points of 1–10 in the process of XAS measurements are indicated. Reference and counter electrode: Li. electrolyte: 1 M $LiPF_6$ in EC/DMC. Temperature: 20°C ± 2°C. On the upper X axis the capacity detected in each step is reported. Reproduced from Ref. [54].

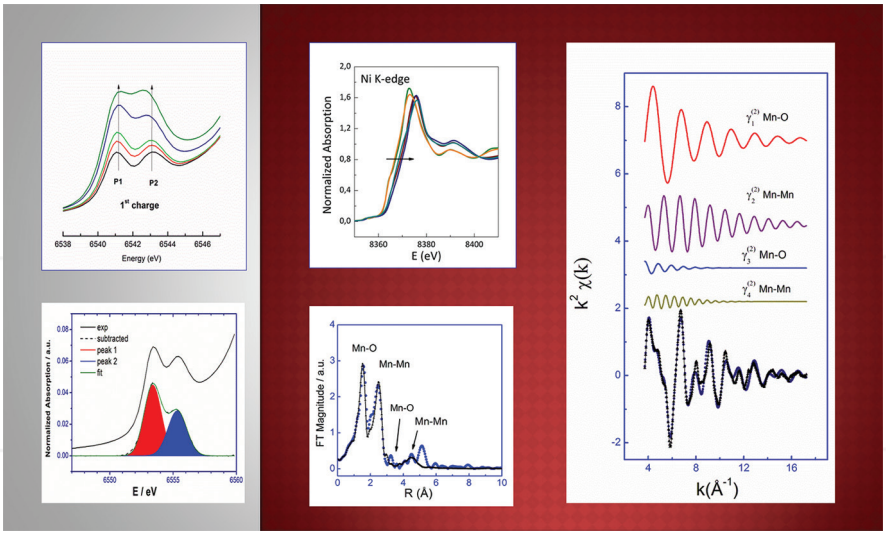

Figure 6. XAS data analysis for the cathode material. The picture displays analysis of the pre-edge data obtained at the Mn K-edge (left panel) including the fitting of the observed peaks (at the bottom). These data provide both charge and symmetry information around the investigated metal. Data at the right panel refer to XANES behavior at the Ni K-edge (up) and the best-fit of the EXAFS data in terms of single contribution to the total EXAFS oscillation (right). At the bottom the fourier transform (FT) behavior of the corresponding EXAFS is displayed. Reproduced from ELETTRA Highlights 2014–15, page 12.

http://dx.doi.org/10.5772/66868

The study here highlighted demonstrates that the manganese is not taking part of the initial electrochemical oxidation process, but a complete Ni^{2+}/Ni^{4+} and a partial Co^{3+}/Co^{4+} redox processes occur during the first charge of the battery. The electrochemical performance of the material, considering the full and partial redox inactivity of Mn and Co, also reveals the participation of oxygen in the overall electrochemical redox process. Analysis of EXAFS at the three metal edges has revealed that the first charge of the lithium-rich cathode can be described by two separate reactions occurring at the two components, Li_2MnO_3 and $LiMO_2$: an activation of the Li_2MnO_3 component with a phase transition to an *hexagonal* layered structure and the oxidation/reduction of both Ni and Co which is not only demonstrated by pre-edge/XANES data but also corroborated by the first shell M-O distances behavior and their corresponding Debye-Waller factors.

4.2. Study of the conversion reaction in electrode materials: the case of $NiSb_2$

A particularly interesting case for the application of *operando* XAS is that of electrode materials undergoing a so-called conversion reaction, which was reviewed a few years ago by Cabana *et al.* [9]. In a conversion reaction, lithium reacts with a binary compound containing a transition metal (M = Ti, Mn, Fe, Co, Ni, etc.) and a group *p* element (X = O, P, Sb, Sn, etc.), according to the following equation:

$$M_a X_b + (b \cdot n)Li \leftrightarrows M + b \cdot Li_n X \tag{9}$$

Conversion reactions were first verified for transition metal oxides [56], but are rather common also for other chalcogenides, pnictogenides and carbon group semimetals. Conversion materials, *i.e.*, materials reacting through the conversion reaction allow reversible capacities as high as 1500 mAh/g, exceeding that of graphite (372 mAh/g), the negative electrode material commonly used in commercial Li-ion batteries. They have thus been considered as possible alternatives for the development of new high-energy storage devices. Recent studies have shown that, for conversion reactions, due to the formation of nanosized species, the composites obtained at the end of discharge are particularly unstable [49] and therefore the use of *operando* techniques for the study of reaction mechanisms is essential. Transition metal antimonides of general formula M_aSb_b form a family of conversion materials providing capacities between 450 and 600 mAh/g and can easily stand up to about 20 cycles at stable capacity before fading. The very large volume expansion (of about 300%) experienced during the reaction with lithium is probably at the origin of the rapid fading, causing the pulverization of the active material particles, with further degradation of the electronic wiring at high-rate and agglomeration of the active mass at low rate [57]. Several methods were used to improve the cycling life of antimonides such as nanostructuration of the electrodes [58], carbon coating and optimization of the formulation [59].

M_aSb_b compounds are expected to react with lithium by forming a matrix of Li_3Sb in which nanoparticles of the transition metal M are embedded. Actual reaction mechanisms, however, can be more complex and often dependent on the specific compound. For instance, several conversion pnictogenides, such as $FeSb_2$ [60] and MnSb [61], form intermediate lithiated insertion phases before starting the veritable conversion reaction, while additional phases could

also form throughout the whole electrochemical cycle. An example of a complicated reaction mechanism is that of $NiSb_2$, which reacts reversibly with lithium to form nickel metal and Li_3Sb providing a theoretical capacity of 532 mAh/g [62].

In this material, the possible formation of an intermediate ternary insertion solid solution was suggested by a slight shift of the XRD reflections during the first part of the discharge [62]. The complete amorphisation of the system during the conversion, however, made it impossible to follow the reaction by XRD. In particular, the formation of Ni nanoparticles at the end of discharge, which are expected for typical conversion reactions, could not be verified. *Operando* Ni K-edge XAS was thus used to address this issue [63].

The EXAFS data collected during the first discharge are shown in **Figure 7**. The fourier transform (FT) signal of pristine $NiSb_2$ exhibits a main contribution with a dominant peak at about 2.4 Å and a second smaller peak slightly below 2 Å, and a second contribution with a dominant peak at 4.2 Å. During lithiation, the first contribution is gradually replaced by a peak pointing at about 2.2 Å, while the peak at 4.2 Å gradually disappears. The spectrum of the fully lithiated material was fitted using 12 Ni neighbors at 2.47(1) Å. This result agrees well with the Ni − Ni distance of 2.491 Å in the *fcc* lattice of Ni metal. Such a fit, however, gives an amplitude reduction factor $S_0^2 = 0.34$, *i.e.*, less than half of the usually observed value. Since S_0^2 is directly correlated to the coordination number, such a low value indicates that the effective number of Ni neighbors is much smaller than 12, in line with the formation of Ni nanoparticles with a significant fraction of surface atoms. Such reduced coordination numbers are often observed for supported metal nanoparticles in heterogeneous catalysts with sizes below about 2 nm [64]. The nanosized nature of the Ni particles is also confirmed by the absence of the following coordination shells in the FT signal. The presence of Ni nanoparticles at the end of lithiation and their following (partial) reaction during delithiation to reform a nanosized form of $NiSb_2$, allowed the author to confirm that $NiSb_2$ is a veritable conversion material.

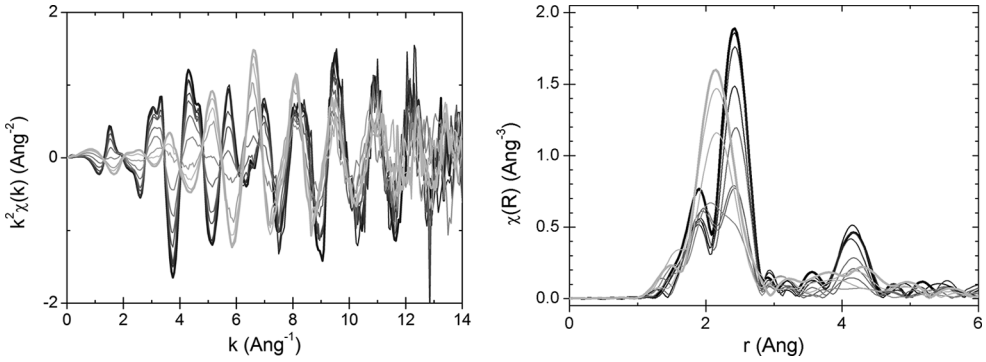

Figure 7. *Operando* evolution of the Ni K-edge EXAFS spectra (left) and corresponding phase-uncorrected FT signals (right) during the first galvanostatic lithiation of $NiSb_2$ vs. Li metal. Evolution with lithiation is shown on going from darker to brighter spectra (only selected spectra are shown for the sake of clearness). Reproduced from Ref. [63].

At the end of this paper, the authors compared the *operando* spectra with those of *ex situ* samples cycled vs. Li about 5 days prior to the XAS measurement campaign, which turned out to be rather different in spite of the precautions taken in order to avoid the decomposition of the latter materials. This comparison underlines the importance of performing *in situ* measurements to get a realistic view of the reaction mechanism of battery materials. In fact, especially in the case of conversion materials, such investigations can be very complex because the species formed in cycling electrodes are usually very reactive and/or unstable.

4.3. Study of Li-sulfur batteries by S K-edge XAS

One of the most interesting recent applications of XAS to electrochemical energy storage concerns the study of lithium-sulfur batteries (LSBs). Since the work of Jie *et al*. [65], many groups have developed first the use of XANES and more recently that of EXAFS for the study of such systems. In LSB, the positive electrode material is elemental sulfur, which can react with lithium to produce Li_2S for a theoretical capacity of 1672 mAh/g at about 2.5 V [66]. The practical capacity of such systems is unfortunately much lower, never exceeding 1200 mAh/g. Moreover, LSB suffer from several other drawbacks: the main one is surely the diffusion of polysulfides (Li_2S_n), produced during the first steps of the reduction of sulfur and highly soluble in the electrolyte, which cause the well-known "shuttle" phenomenon strongly limiting the capacity [67]. Second, solid Li_2S and elemental sulfur are both insulating and cannot be used as such in normal composite electrodes, fabricated as mixtures of sulfur and carbon powder on aluminum foil current collectors, since their continuous dissolution/precipitation during cycling gradually disconnects part of the active mass, making sulfur progressively electrochemically inactive [68, 69]. All these disadvantages cause rapid capacity fading and low columbic efficiency of LSB.

Several improvements have been suggested in the last years to tackle these drawbacks: one of them consisted in infiltrating molten sulfur into porous conductive carbon materials [70]. This approach, however, does not allow large sulfur loadings, nor does it prevent the diffusion of polysulfides outside the pores. Moreover, it requires large amounts of electrolyte to wet the large volume of porous carbon and to solubilize the polysulfides, which greatly reduces the volumetric energy density of LSB. Most recently, multifunctional positive electrodes, enhancing the sulfur loading and promoting the interaction of polysulfides with the electrode host to prevent their diffusion in the electrolyte have been successfully proposed and studied [71]. In all these studies, XAS has been largely used at different levels to investigate in detail the electrochemical mechanism and the diffusion (or retention) of polysulfides as well as the possible different failure paths.

Sulfur K-edge XANES, for instance, can be used as a semiquantitative analytical tool for LSB [72–81]. *Operando* XANES spectra fitted by linear combinations of reference XANES spectra of pure sulfur, synthetic polysulfides and Li_2S allowed following both the evolution of the sulfur species and of their relative ratio along the discharge and the charge process, as well as the variation of the concentration of sulfur in both the cathode and the electrolyte, in line with the diffusion of the polysulfides in the whole battery. More recently, it was also used for the detection of the formation of sulfur radical species [82–84], which were confirmed also by *operando* Raman spectroscopy [53].

A particularly interesting approach was, however, the application of EXAFS to the study of the electrochemical mechanism [85]. Such study was possible only due to the use of a specific sulfur-free electrolyte salt, which usually hindered the EXAFS contribution of the sulfur species evolving during cycling (cf. **Figure 8**). In this way, it was possible to clearly identify the type of polysulfides (long- or short-chain) formed in the electrode during the high-voltage and the low-voltage discharge plateaus and to confirm the formation of Li_2S only from the beginning of the low-voltage plateau and to follow its concentration in the electrode.

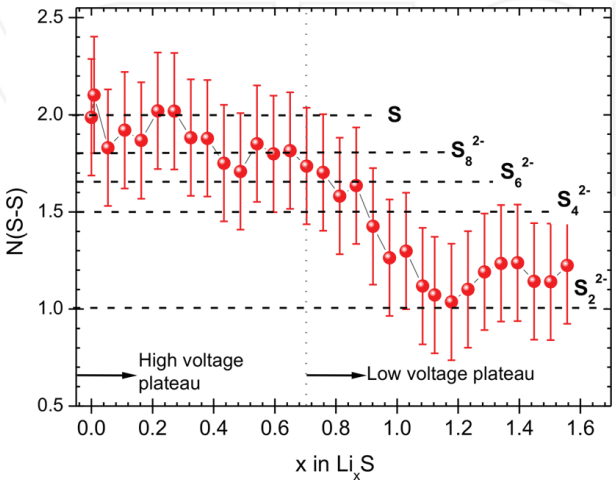

Figure 8. Variation of the average *S* coordination number during the first discharge. The average coordination of the most important polysulfides is reported for comparison. The vertical line represents the end of the high-voltage plateau. From Ref. [85].

Finally, XAS was very recently used for detecting the interaction of sulfur precursors with appropriately modified graphene oxide nanocomposites, leading to the immobilization of the sulfur species in the electrode, improving the overall cycling performance of the cell [86].

All these examples underlined the powerful properties of XAS for the *operando* study of electrochemical mechanisms in batteries even at low energies (sulfur K-edge is at only 2.47 keV).

5. The chemometric approach to the interpretation of XAS data

Due to the increasing performance of many synchrotron beamlines specialized in *in situ* XAS studies, extremely large dataset containing many tens or hundreds of spectra associates to a single experiment are currently collected. This huge amount of data is calling for a suitable strategy for their treatment in reasonable time. For instance, the study of the charge or the discharge process of a battery produces something like 100–300 spectra, depending on the experimental conditions (data acquisition protocol and battery discharge rate). In similar cases, the

use of chemometrics may be applied [87]. Specifically, the application of multivariate curve resolution (MCR) to large datasets of *in situ* XAS experiments (where the samples undergo continuous evolution during the reaction path) allows one to interpret their modification in terms of sums of pure spectra with variable concentration profiles, without needing any pre-existing model or *a priori* information about the system. To our knowledge, the first application of MRC to a XAS study of battery materials concerns the investigation of the evolution during charge of a positive electrode based on a $Cu_{0.1}V_2O_5$ xerogel [40]. This study, which is performed using the alternate least square (ALS) algorithm, allowed obtaining relevant information on the cell charging dynamics. In particular, the data treatment evidenced for the first time the occurrence of three species during the battery charging, which were further identified with a common EXAFS analysis. This successful chemometric approach to XAS has further been used for other *operando* studies, mostly by the catalysis community [88]. MCR was also applied to analyze XAS data from Fischer-Tropsch reaction [89] and to infer about the speciation and the evolution of ruthenium in Co − Ru/SiO2 systems by looking at quick-XAS data [90].

6. Perspectives

With the increasing demand of energy resources for both portable and storage purposes, there has been an extensive and increasingly diversification of materials and technology for the electrochemical power sources in the last five years. Not only lithium-ion technology but also sodium or even trivalent ions, also in aqueous media, are currently studied to obtain a good balancing between cost, safety, abundance and electrochemical performances. This chapter has underlined the strength of the XAFS probe to understand the dynamic of the both anode and cathode materials during the battery functioning, at atomic level. We feel that this core-level spectroscopy can even meet the increasing demand of deep understanding of different technologies and of new materials for batteries. This extraordinary versatility is due to: (i) the extremely selective local structure probe of XAS for the atomic species in crystalline, amorphous solid and liquid electrolyte; (ii) the unprecedented quality and speed of for data recording in synchrotron beamlines dedicated to *in situ* studies, coupled with a suitable and unbiased data analysis such as the chemometric approach to XAFS data presented above; (iii) the new generations of software for EXAFS data analysis, which are capable of analyzing multiple scattering contributions with great efficiency and to perform simultaneous multiple edge fits; (iv) the development of reliable spectrometers at synchrotron radiation light sources enabling high resolution recording, allowing the collection of complementary information with ancillary advanced techniques such as resonant inelastic X-ray scattering (RIXS) [91].

Moreover, new advanced synchrotron-based techniques are expected to be at the forefront of battery research in the future; among them, there will surely be X-ray transmission microscopy, which allows the simultaneous imaging and spatially resolved XAS study of electrode materials in batteries [92].

Finally, a personal consideration: in XAS, data analysis is usually considered as the bottleneck of the whole spectroscopic study. This holds true regardless of the simplicity or the difficulty of the oscillatory portion of the spectrum to be analyzed. Indeed, as long as a suitable struc-

tural model has not been established, an oscillation can be interpreted in several different ways. It is then recommended to newcomers not only to learn how to conduct XAS experiments, but also to perform appropriate data analyses by seeking the advice and collaboration of experts who are willing to share their knowledge and their experience.

Acknowledgements

Work supported by RFO funding (University of Bologna). Thanks are due to staff at both Sincrotrone Trieste and Synchrotron SOLEIL for assistance during the experiments and for providing synchrotron radiation.

Author details

Marco Giorgetti[1]* and Lorenzo Stievano[2]

*Address all correspondence to: marco.giorgetti@unibo.it

1 Department of Industrial Chemistry "Toso Montanari", University of Bologna, Bologna, Italy

2 Institut Charles Gerhardt – AIME, University of Montpellier, Montpellier, France

References

[1] Dunn, B., Kamath, H., Tarascon, J.-M.: Electrical Energy Storage for the Grid: A Battery of Choices. Science. 334, 928–935 (2011).

[2] Vincent, C.A., Scrosati, B.: Modern Batteries—An Introduction to Electrochemical Power Sources—2nd Edition. Butterworth-Heinemann, Oxford, UK (1997).

[3] Wagemaker, M., Mulder, F.M.: Properties and Promises of Nanosized Insertion Materials for Li-Ion Batteries. Acc. Chem. Res. 46, 1206–1215 (2013).

[4] Masquelier, C., Croguennec, L.: Polyanionic (Phosphates, Silicates, Sulfates) Frameworks as Electrode Materials for Rechargeable Li (or Na) Batteries. Chem. Rev. 113, 6552–6591 (2013).

[5] Whittingham, M.S.: Lithium Batteries and Cathode Materials. Chem. Rev. 104, 4271–4302 (2004).

[6] Obrovac, M.N., Chevrier, V.L.: Alloy Negative Electrodes for Li-Ion Batteries. Chem. Rev. 114, 11444–11502 (2014).

[7] Kim, H., Jeong, G., Kim, Y.-U., Kim, J.-H., Park, C.-M., Sohn, H.-J.: Metallic Anodes for Next Generation Secondary Batteries. Chem. Soc. Rev. 42, 9011–9034 (2013).

[8] Park, C.-M., Kim, J.-H., Kim, H., Sohn, H.-J.: Li-Alloy Based Anode Materials for Li Secondary Batteries. Chem. Soc. Rev. 39, 3115–3141 (2010).

[9] Cabana, J., Monconduit, L., Larcher, D., Palacín, M.R.: Beyond Intercalation-Based Li-Ion Batteries: The State of the Art and Challenges of Electrode Materials Reacting Through Conversion Reactions. Adv. Mater. 22, E170–E192 (2010).

[10] Peled, E.: The Electrochemical Behavior of Alkali and Alkaline Earth Metals in Nonaqueous Battery Systems—The Solid Electrolyte Interphase Model. J. Electrochem. Soc. 126, 2047–2051 (1979).

[11] Sharma, N., Pang, W.K., Guo, Z., Peterson, V.K.: In Situ Powder Diffraction Studies of Electrode Materials in Rechargeable Batteries. ChemSusChem. 8, 2826–2853 (2015).

[12] Li, J.-T., Zhou, Z.-Y., Broadwell, I., Sun, S.: In-Situ Infrared Spectroscopic Studies of Electrochemical Energy Conversion and Storage. Acc. Chem. Res. 45, 485–494 (2012).

[13] Baddour-Hadjean, R., Pereira-Ramos, J.-P.: Raman Microspectrometry Applied to the Study of Electrode Materials for Lithium Batteries. Chem. Rev. 110, 1278–1319 (2010).

[14] Lippens, P.-E., Jumas, J.-C.: Mössbauer Spectroscopy Investigation of Batteries. Mössbauer Eff. Ref. Data J. 33, 31 (2010).

[15] Martha, S.K., Markevich, E., Burgel, V., Salitra, G., Zinigrad, E., Markovsky, B., Sclar, H., Pramovich, Z., Heik, O., Aurbach, D., Exnar, I., Buqa, H., Drezen, T., Semrau, G., Schmidt, M., Kovacheva, D., Saliyski, N.: A Short Review on Surface Chemical Aspects of Li Batteries: A Key for a Good Performance. J. Power Sources. 189, 288–296 (2009).

[16] Verma, P., Maire, P., Novák, P.: A Review of the Features and Analyses of the Solid Electrolyte Interphase in Li-Ion Batteries. Electrochim. Acta. 55, 6332–6341 (2010).

[17] McBreen, J., O'Grady, W.E., Pandya, K.I.: EXAFS: A New Tool for the Study of Battery and Fuel Cell Materials. J. Power Sources. 22, 323–340 (1988).

[18] Giorgetti, M.: A Review on the Structural Studies of Batteries and Host Materials by X-Ray Absorption Spectroscopy. ISRN Mater. Sci. 2013, 938625 (2013).

[19] Shearing, P., Wu, Y., Harris, S.J., Brandon, N.: In Situ X-Ray Spectroscopy and Imaging of Battery Materials. Electrochem. Soc. Interface. 20, 43–47 (2011).

[20] Croy, J.R., Balasubramanian, M., Kim, D., Kang, S.-H., Thackeray, M.M.: Designing High-Capacity, Lithium-Ion Cathodes Using X-ray Absorption Spectroscopy. Chem. Mater. 23, 5415–5424 (2011).

[21] Balasubramanian, M., Sun, X., Yang, X.Q., McBreen, J.: In Situ X-Ray Diffraction and X-Ray Absorption Studies of High-Rate Lithium-Ion Batteries. J. Power Sources. 92, 1–8 (2001).

[22] Filipponi, A.: EXAFS for liquids. J. Physi.: Condens. Matter. 13, R23–R60 (2001).

[23] Niemantsverdriet, J.W.: Spectroscopy in Catalysis. Wiley-VCH, Weinheim (1995).

[24] Nelson, R.C., Miller, J.T.: An Introduction to X-Ray Absorption Spectroscopy and its In Situ Application to Organometallic Compounds and Homogeneous Catalysts. Catal. Sci. Technol. 2, 461–470 (2012).

[25] Carrier, X., Marceau, E., Carabineiro, H., Rodríguez-González, V., Che, M.: EXAFS Spectroscopy as a Tool to Probe Metal–Support Interaction and Surface Molecular Structures in Oxide-Supported Catalysts: Application to Al_2O_3-Supported Ni(II) Complexes and ZrO_2-Supported Tungstates. Phys. Chem. Chem. Phys. 11, 7527–7539 (2009).

[26] Ascone, I., Fourme, R., Hasnain, S.S.: Introductory Overview: X-Ray Absorption Spectroscopy and Structural Genomics. J. Synchrotron Radiat. 10, 1–3 (2003).

[27] Solomon, E.I.: Synchrotron Radiation in Inorganic and Bioinorganic Chemistry: Preface. Coord. Chem. Rev. 249, 1–2 (2005).

[28] Dewald, H.D.: Use of EXAFS to Probe Electrode-Solution Interfaces. Electroanal. 3, 145–155 (1991).

[29] Teo, B.K.: EXAFS: Basic Principles and Data Analysis. Springer Berlin-Heidelberg, Berlin, Heidelberg, Germany (1986).

[30] Koningsberger, D.C., Prins, R.: X-Ray Absorption : Principles, Applications, Techniques of EXAFS, SEXAFS, and XANES. Wiley Interscience, New York, USA (1988).

[31] van Bokhoven, J.A., Lamberti, C.: X-Ray Absorption and X-Ray Emission Spectroscopy : Theory and Applications. John Wiley & Sons Ltd., Chichester, UK (2016).

[32] Bunker, G.: Introduction to XAFS, A Practical Guide to X-Ray Absorption Fine Structure Spectroscopy. Cambridge University Press, Cambridge, UK (2010).

[33] Filipponi, A., Di Cicco, A.: X-Ray-Absorption Spectroscopy and N-Body Distribution Functions in Condensed Matter. II. Data Analysis and Applications. Phys. Rev. B. 52, 15135–15149 (1995).

[34] Ankudinov, A.L., Ravel, B., Rehr, J.J., Conradson, S.D.: Real-Space Multiple-Scattering Calculation and Interpretation of X-Ray-Absorption Near-Edge Structure. Phys. Rev. B. 58, 7565–7576 (1998).

[35] Rehr, J.J., Kas, J.J., Vila, F.D., Prange, M.P., Jorissen, K.: Parameter-Free Calculations of X-Ray Spectra with FEFF9. Phys. Chem. Chem. Phys. 12, 5503–5513 (2010).

[36] Tomic, S., Searle, B.G., Wander, A., Harrison, N.M., Dent, A.J., Mosselmans, J.F.W., Inglesfield, J.E.: New Tools for the Analysis of EXAFS: The DL EXCURV Package. (2004).

[37] Newville, M.: IFEFFIT : Interactive XAFS Analysis and FEFF Fitting. J. Synchrotron Radiat. 8, 322–324 (2001).

[38] Ravel, B., Newville, M.: ATHENA, ARTEMIS, HEPHAESTUS: Data analysis for X-Ray Absorption Spectroscopy Using IFEFFIT. J. Synchrotron Radiat. 12, 537–541 (2005).

[39] Giorgetti, M., Aquilanti, G., Ballarin, B., Berrettoni, M., Cassani, M.C., Fazzini, S., Nanni, D., Tonelli, D.: Speciation of Gold Nanoparticles by Ex Situ Extended X-ray Absorption Fine Structure and X-Ray Absorption Near Edge Structure. Anal. Chem. 88, 6873–6880 (2016).

[40] Conti, P., Zamponi, S., Giorgetti, M., Berrettoni, M., Smyrl, W.H.: Multivariate Curve Resolution Analysis for Interpretation of Dynamic Cu K-Edge X-Ray Absorption Spectroscopy Spectra for a Cu Doped V_2O_5 Lithium Battery. Anal. Chem. 82, 3629–3635 (2010).

[41] Boscherini, F.: Applications of XAFS to Nanostructures and Materials Science. In: Settimio Mobilio, Federico Boscherini, C.M. (ed.) Synchrotron Radiation. pp. 485–498. Springer Berlin-Heidelberg, Berlin, Heidelberg (2015).

[42] Guda, A.A., Soldatov, M.A., Soldatov, A. V.: Group III–V and II–VI Quantum Dots and Nanoparticles. In: Schnohr, C.S. and Ridgway, M.C. (eds.) X-Ray Absorption Spectroscopy of Semiconductors. pp. 247–268. Springer Berlin-Heidelberg, Berlin, Germany (2015).

[43] Frenkel, A.I., Hills, C.W., Nuzzo, R.G.: A View from the Inside: Complexity in the Atomic Scale Ordering of Supported Metal Nanoparticles. J. Phys. Chem. B. 105, 12689–12703 (2001).

[44] de Groot, F., Vankó, G., Glatzel, P.: The 1s X-Ray Absorption Pre-Edge Structures in Transition Metal Oxides. J. Phys. Condens. Matter. 21, 104207 (2009).

[45] Westre, T.E., Kennepohl, P., DeWitt, J.G., Hedman, B., Hodgson, K.O., Solomon, E.I.: A Multiplet Analysis of Fe K-Edge 1s → 3d Pre-Edge Features of Iron Complexes. J. Am. Chem. Soc. 119, 6297–6314 (1997).

[46] Benfatto, M., Della Longa, S., Natoli, C.R.: The MXAN procedure: a new method for analysing the XANES spectra of metalloproteins to obtain structural quantitative information. J. Synchrotron Radiat. 10, 51–57 (2003).

[47] Joly, Y.: X-Ray Absorption Near-Edge Structure Calculations Beyond the Muffin-Tin Approximation. Phys. Rev. B. 63, 125120 (2001).

[48] Stavitski, E., de Groot, F.M.F.: The CTM4XAS Program for EELS and XAS Spectral Shape Analysis of Transition Metal L Edges. Micron. 41, 687–694 (2010).

[49] Johnston, K.E., Sougrati, M.T., Stievano, L., Darwiche, A., Dupré, N., Grey, C.P., Monconduit, L.: Effects of Relaxation on Conversion Negative Electrode Materials for Li-Ion Batteries: A Study of TiSnSb Using 119 Sn Mössbauer and 7 Li MAS NMR Spectroscopies. Chem. Mater. 28, 4032–4041 (2016).

[50] Leriche, J.-B., Hamelet, S., Shu, J., Morcrette, M., Masquelier, C., Ouvrard, G., Zerrouki, M., Soudan, P., Belin, S., Elkaïm, E., Baudelet, F.: An Electrochemical Cell for Operando Study of Lithium Batteries Using Synchrotron Radiation. J. Electrochem. Soc. 157, A606–A610 (2010).

[51] Conte, D.E., Mouyane, M., Stievano, L., Fraisse, B., Sougrati, M.T., Olivier-Fourcade, J., Willmann, P., Jordy, C., Artus, M., Cassaignon, S., Driezen, K., Jumas, J.-C.: A Combined Mössbauer Spectroscopy and X-Ray Diffraction Operando Study of Sn-Based Composite Anode Materials for Li-Ion Accumulators. J. Solid State Electrochem. 16, 3837–3848 (2012).

[52] Sougrati, M.T., Fullenwarth, J., Debenedetti, A., Fraisse, B., Jumas, J.-C., Monconduit, L.: TiSnSb a New Efficient Negative Electrode for Li-Ion Batteries: Mechanism Investigations by Operando-XRD and Mössbauer Techniques. J. Mater. Chem. 21, 10069–10076 (2011).

[53] Hannauer, J., Scheers, J., Fullenwarth, J., Fraisse, B., Stievano, L., Johansson, P.: The Quest for Polysulfides in Lithium-Sulfur Battery Electrolytes: An Operando Confocal Raman Spectroscopy Study. ChemPhysChem. 16, 2755–2759 (2015).

[54] Buchholz, D., Li, J., Passerini, S., Aquilanti, G., Wang, D., Giorgetti, M., Capacity, H.: X-Ray Absorption Spectroscopy Investigation of Lithium-Rich, Cobalt-Poor Layered-Oxide Cathode Material with High Capacity. ChemElectroChem. 2, 85–97 (2015).

[55] Giorgetti, M., Wang, D., Aquilanti, G., Buchholz, D., Passerini, S.: Local Structure Modification in Lithium Rich Layered Li-Mn-O Cathode Material. J. Phys.: Conf. Ser. 712, 12130 (2016).

[56] Poizot, P., Laruelle, S., Grugeon, S., Dupont, L., Tarascon, J.-M.: Nano-Sized Transition-Metal Oxides as Negative-Electrode Materials for Lithium-Ion Batteries. Nature. 407, 496–499 (2000).

[57] Marino, C., Fullenwarth, J., Monconduit, L., Lestriez, B.: Diagnostic of the Failure Mechanism in $NiSb_2$ Electrode for Li Battery through Analysis of its Polarization on Galvanostatic Cycling. Electrochim. Acta. 78, 177–182 (2012).

[58] Villevieille, C., Ionica-Bousquet, C.M., De Benedetti, A., Morato, F., Pierson, J.-F., Simon, P., Monconduit, L.: Self Supported Nickel Antimonides Based Electrodes for Li Ion Battery. Solid State Ionics. 192, 298–303 (2011).

[59] Sivasankaran, V., Marino, C., Chamas, M., Soudan, P., Guyomard, D., Jumas, J.-C., Lippens, P.-E., Monconduit, L., Lestriez, B.: Improvement of Intermetallics Electrochemical Behavior by Playing With the Composite Electrode Formulation. J. Mater. Chem. 21, 5076–5082 (2011).

[60] Villevieille, C., Fraisse, B., Womes, M., Jumas, J.-C., Monconduit, L.: A New Ternary Li_4FeSb_2 Structure Formed upon Discharge of the $FeSb_2$/Li Cell. J. Power Sources. 189, 324–330 (2009).

[61] Fransson, L.M.L., Vaughey, J.T., Edström, K., Thackeray, M.M.: Structural Transformations in Intermetallic Electrodes for Lithium Batteries. J. Electrochem. Soc. 150, A86 (2003).

[62] Villevieille, C., Ionica-Bousquet, C.M., Ducourant, B., Jumas, J.-C., Monconduit, L.: $NiSb_2$ as Negative Electrode for Li-Ion Batteries: An Original Conversion Reaction. J. Power Sources. 172, 388–394 (2007).

[63] Marino, C., Fraisse, B., Womes, M., Villevieille, C., Monconduit, L., Stievano, L.: At the Heart of a Conversion Reaction: An Operando X-Ray Absorption Spectroscopy Investigation of $NiSb_2$, a Negative Electrode Material for Li-Ion Batteries. J. Phys. Chem. C. 118, 27772–27780 (2014).

[64] Greegor, R.B., Lytle, F.W.: Morphology of supported metal clusters: Determination by EXAFS and chemisorption. J. Catal. 63, 476–486 (1980).

[65] Gao, J., Lowe, M.A., Kiya, Y., Abruña, H.D.: The Effects of Liquid Electrolytes on the Charge-Discharge Performance of Rechargeable Lithium/Sulfur Batteries: Electrochemical and In-Situ X-Ray Absorption Spectroscopic Studies. J. Phys. Chem. C. 115, 25132–25137 (2011).

[66] Bruce, P.G., Freunberger, S.A., Hardwick, L.J., Tarascon, J.-M.: Li–O_2 and Li–S Batteries with High Energy Storage. Nat. Mater. 11, 19–29 (2011).

[67] Mikhaylik, Y.V., Akridge, J.R.: Low Temperature Performance of Li/S Batteries. J. Electrochem. Soc. 150, A306–A311 (2003).

[68] Cheon, S.-E., Ko, K.-S., Cho, J.-H., Kim, S.-W., Chin, E.-Y., Kim, H.-T.: Rechargeable Lithium Sulfur Battery: I. Structural Change of Sulfur Cathode During Discharge and Charge. J. Electrochem. Soc. 150, A796–A799 (2003).

[69] Cheon, S.-E., Ko, K.-S., Cho, J.-H., Kim, S.-W., Chin, E.-Y., Kim, H.-T.: Rechargeable Lithium Sulfur Battery: II. Rate Capability and Cycle Characteristics. J. Electrochem. Soc. 150, A800–A805 (2003).

[70] Choi, N.-S., Chen, Z., Freunberger, S.A., Ji, X., Sun, Y.-K., Amine, K., Yushin, G., Nazar, L.F., Cho, J., Bruce, P.G.: Challenges Facing Lithium Batteries and Electrical Double-Layer Capacitors. Angew. Chem. Int. Ed. 51, 9994–10024 (2012).

[71] Pang, Q., Liang, X., Kwok, C.Y., Nazar, L.F.: Advances in Lithium–Sulfur Batteries Based on Multifunctional Cathodes and Electrolytes. Nat. Energy. 1, 16132 (2016).

[72] Patel, M.U.M., Arčon, I., Aquilanti, G., Stievano, L., Mali, G., Dominko, R.: X-Ray Absorption Near-Edge Structure and Nuclear Magnetic Resonance Study of the Lithium-Sulfur Battery and its Components. ChemPhysChem. 15, 894–904 (2014).

[73] Cuisinier, M., Cabelguen, P.-E., Evers, S., He, G., Kolbeck, M., Garsuch, A., Bolin, T., Balasubramanian, M., Nazar, L.F.: Sulfur Speciation in Li–S Batteries Determined by Operando X-ray Absorption Spectroscopy. J. Phys. Chem. Lett. 4, 3227–3232 (2013).

[74] Pascal, T.A., Wujcik, K.H., Velasco-Velez, J., Wu, C., Teran, A.A., Kapilashrami, M., Cabana, J., Guo, J., Salmeron, M., Balsara, N., Prendergast, D.: X-ray Absorption Spectra of Dissolved Polysulfides in Lithium–Sulfur Batteries from First-Principles. J. Phys. Chem. Lett. 5, 1547–1551 (2014).

[75] Cuisinier, M., Cabelguen, P.-E., Adams, B.D., Garsuch, A., Balasubramanian, M., Nazar, L.F.: Unique Behaviour of Nonsolvents for Polysulphides in Lithium–Sulphur Batteries. Energy Environ. Sci. 7, 2697–2705 (2014).

[76] Lowe, M.A., Gao, J., Abruña, H.D.: Mechanistic Insights into Operational Lithium–Sulfur Batteries by In Situ X-Ray Diffraction and Absorption Spectroscopy. RSC Adv. 4, 18347–18353 (2014).

[77] Yu, X., Pan, H., Zhou, Y., Northrup, P., Xiao, J., Bak, S., Liu, M., Nam, K.-W., Qu, D., Liu, J., Wu, T., Yang, X.-Q.: Direct Observation of the Redistribution of Sulfur and Polysulfides in Li-S Batteries During the First Cycle by In Situ X-Ray Fluorescence Microscopy. Adv. Energy Mater. 5, 1500072 (2015).

[78] Pang, Q., Kundu, D., Cuisinier, M., Nazar, L.F.: Surface-Enhanced Redox Chemistry of Polysulphides on a Metallic and Polar Host for Lithium-Sulphur Batteries. Nat. Commun. 5, 4759 (2014).

[79] Vijayakumar, M., Govind, N., Walter, E., Burton, S.D., Shukla, A., Devaraj, A., Xiao, J., Liu, J., Wang, C., Karim, A., Thevuthasan, S.: Molecular Structure and Stability of Dissolved Lithium Polysulfide Species. Phys. Chem. Chem. Phys. 16, 10923–10932 (2014).

[80] Zhu, P., Song, J., Lv, D., Wang, D., Jaye, C., Fischer, D.A., Wu, T., Chen, Y.: Mechanism of Enhanced Carbon Cathode Performance by Nitrogen Doping in Lithium–Sulfur Battery: An X-Ray Absorption Spectroscopic Study. J. Phys. Chem. C. 118, 7765–7771 (2014).

[81] Gorlin, Y., Siebel, A., Piana, M., Huthwelker, T., Jha, H., Monsch, G., Kraus, F., Gasteiger, H.A., Tromp, M.: Operando Characterization of Intermediates Produced in a Lithium-Sulfur Battery. J. Electrochem. Soc. 162, A1146–A1155 (2015).

[82] Pascal, T.A., Pemmaraju, C.D., Prendergast, D.: X-Ray Spectroscopy as a Probe for Lithium Polysulfide Radicals. Phys. Chem. Chem. Phys. 17, 7743–7753 (2015).

[83] Wujcik, K.H., Pascal, T.A., Pemmaraju, C.D., Devaux, D., Stolte, W.C., Balsara, N.P., Prendergast, D.: Characterization of Polysulfide Radicals Present in an Ether-Based Electrolyte of a Lithium-Sulfur Battery During Initial Discharge Using In Situ X-Ray Absorption Spectroscopy Experiments and First-Principles Calculations. Adv. Energy Mater. 5, 1500285 (2015).

[84] Cuisinier, M., Hart, C., Balasubramanian, M., Garsuch, A., Nazar, L.F.: Radical or Not Radical : Revisiting Lithium—Sulfur Electrochemistry in Nonaqueous Electrolytes. Adv. Energy Mater. 5, 1401801 (2015).

[85] Dominko, R., Patel, M.U.M., Lapornik, V., Vizintin, A., Koželj, M., Novak Tušar, N., Arcon, I., Stievano, L., Aquilanti, G.: Analytical Detection of Polysulfides in the Presence of Adsorption Additives by Operando X-Ray Absorption Spectroscopy. J. Phys. Chem. C. 119, 19001–19010 (2015).

[86] Ye, Y., Kawase, A., Song, M.-K., Feng, B., Liu, Y.-S., Marcus, M.A., Feng, J., Fang, H., Cairns, E.J., Zhu, J., Guo, J.: X-Ray Absorption Spectroscopic Characterization of the Synthesis Process: Revealing the Interactions in Cetyltrimethylammonium Bromide-Modified Sulfur–Graphene Oxide Nanocomposites. J. Phys. Chem. C. 120, 10111–10117 (2016).

[87] de Juan, A., Jaumot, J., Tauler, R.: Multivariate Curve Resolution (MCR). Solving the Mixture Analysis Problem. Anal. Methods. 6, 4964 (2014).

[88] Cassinelli, W.H., Martins, L., Passos, A.R., Pulcinelli, S.H., Santilli, C. V., Rochet, A., Briois, V.: Multivariate curve resolution analysis applied to time-resolved synchrotron X-ray Absorption Spectroscopy monitoring of the activation of copper alumina catalyst. Catal. Today. 229, 114–122 (2014).

[89] Voronov, A., Urakawa, A., van Beek, W., Tsakoumis, N.E., Emerich, H., Rønning, M.: Multivariate Curve Resolution Applied to In Situ X-Ray Absorption Spectroscopy Data: An Efficient Tool for Data Processing and Analysis. Anal. Chim. Acta. 840, 20–27 (2014).

[90] Hong, J., Marceau, E., Khodakov, A.Y., Gaberová, L., Griboval-Constant, A., Girardon, J.-S., La Fontaine, C., Briois, V.: Speciation of Ruthenium as a Reduction Promoter of Silica-Supported Co Catalysts: A Time-Resolved In Situ XAS Investigation. ACS Catal. 5, 1273–1282 (2015).

[91] Ament, L.J.P., van Veenendaal, M., Devereaux, T.P., Hill, J.P., van den Brink, J.: Resonant Inelastic X-Ray Scattering Studies of Elementary Excitations. Rev. Mod. Phys. 83, 705–767 (2011).

[92] Olivares-Marín, M., Sorrentino, A., Lee, R.-C., Pereiro, E., Wu, N.-L., Tonti, D.: Spatial Distributions of Discharged Products of Lithium-Oxygen Batteries Revealed by Synchrotron X-ray Transmission Microscopy. Nano Lett. 15, 6932–6938 (2015).

INTECH